POROUS METAL OXIDE-CARBON COMPOSITE WITH HOLLOW STRUCTURE FOR ENERGY STORAGE APPLICATIONS

Surya Prasad Adhikari[*1]

ABSTRACT

Nanocomposite structure of porous hollow TiO_2 nanofibers (NFs) and graphitic carbon nitride (g-C_3N_4) sheets were directly fabricated by means of a novel electrospinning combined with calcination process. Owing to the high porosity, these nanostructured demonstrate enhanced energy storage properties when used in supercapacitors (SCs). Nanomaterials in particular offer unique properties or combinations of properties as electrodes and electrolytes in a range of energy devices. The energy storage behavior of electrochemical capacitors (ECs) made from TiO_2/g-C_3N_4 nanocomposites was investigated by cyclic voltammetry and electrochemical impedance spectra. These tests showed that the supercapacitive performance of g-C_3N_4 was significantly enhanced after attaching porous TiO_2 nanofibers.

Keywords: *Electrospinning, g-C_3N_4, Porous TiO_2 NFs, Supercapacitors*

INTRODUCTION

Because of the dazzling advantages of SCs, such as short operating time of charge and discharge, long cycle life, relatively high energy density, and power density devices, SCs are replacing environmentally harmful fuels in more and more fields [1, 2] . However, some shortcomings still need to be solved including the high cost, instability and low energy density; the key to solving these problems is the electrode materials [3]. SCs are prepared from carbon-based materials including activated carbon, carbide derived carbon, zeolite-templated carbon, carbon aerogel, carbon nanotube, onion-like carbon, carbon fiber, grapheme and graphitic carbon nitride (g-C_3N_4) [4-6]. Among these materials, Graphitic carbon nitride (g-C3N4), a polymeric, metal-free, non toxic, earth-abundant and visible light driven semiconductor with a mild band gap (2.7 eV) has become hot-spot in various scientific exploits such as environmental pollution mitigation, energy generation and storage, organic synthesis, sensors, etc due to the tri-s-triazine units that are connected by amino groups in each layer and the weak van der waals forces between layers [3, 7]. Most of the published article can be found mainly focusing on catalytic applications of g-C_3N_4. However, a systematic description of the energy-related applications such as batteries, SCs, white-light-emitting diodes, and oxygen reduction reaction of g-C_3N_4 has not been presented until now. The presence of nitrogen atoms in the graphene-like layered g-C_3N_4 structure gives high supercapacitive performance with better performance than graphene in some aspect [8, 9]. However, the supercapacitive efficiency of g-C_3N_4 alone is still low due to its lower practical surface area. So, various techniques have been adopted

[1] *Department of Automobile & Mechanical Engineering*
Thapathali Campus, Institute of Engineering, Nepal
[*] *Corresponding author*
E-mail : surya@tcioe.edu.np

to improve its capacitive efficiency. The fabrication of composite materials with other semiconductors, doping with noble metals and non-metals are worth mentioning [10-12].

Metal oxides such as nickel oxide, cobalt oxide, zinc oxide, titanium oxide and manganese oxide etc., have been used widely in SCs because of its high specific capacitance and prominent electrochemical properties. Among these, TiO_2 has found to be a gifted and competent metal oxide because of its considerable advantages such as low cost, chemically stable, natural abundance, low toxicity, environmentally friendly nature, good dielectric materials and faradic capacitance [13, 14]. It has wide application, such as, catalysis, ion-sieves, rechargeable batteries, chemical sensing devices, magnetic devices, field-emission devices, hydrogen storage media, electrochemical capacitors and microelectronics. [15-19].

The merged TiO_2 with g-C_3N_4 sheets has expected to form a composite material with high capacitance from the above mention articles. The practical applications of any composites depend on the morphology. Therefore TiO_2/g-C_3N_4 composite is also unalterably depending on the morphology of these two materials. The biggest challenge is to control the structure of these composites. Previous literature has reported that the sheet-like structures of g-C_3N_4-based composites exhibit distinctive optical and electronics properties compared to bulk g-C_3N_4 composites [20]. Similarly, among various TiO_2 nanostructures, the one-dimensional TiO_2 NFs or nanorods attracted serious interest in view of the dimensional confinement and minimal agglomeration compared to nanoparticles (NPs) [21]. Therefore, bearing in mind the above mentioned observations, it is to be predicted that a composite made of sheet-like g-C_3N_4 and porous TiO_2 NFs will exhibit encouraging properties, tending toward-enhanced electrochemical properties. So, I am inspired to develop a simple technique for creating such a composite material. To the best of my knowledge, there has been no report on the fabrication of one dimensional porous TiO_2 NFs grafted onto g-C_3N_4 sheets. Recently, Han C. et al. synthesized a composite of TiO_2 NFs and g-C_3N_4 sheets by electrospinning, in which g-C_3N_4 was embedded inside the NFs [22]. But, in this study, for the first time, TiO_2 porous NFs-having sufficient length were dispersed homogeneously and attached on the surfaces of g-C_3N_4 sheet, with minimal agglomeration of NFs from an angled two-nozzle electrospinning process with calcination. Here, the massive surface area of g-C_3N_4 sheets provides satisfactory surfaces for the direct attachment of TiO_2 NFs, which make charge separation more efficient. Such NFs have a better chance than NPs to be uniformly attached onto g-C_3N_4 sheets to form bonding, simply based on geometric considerations. Thus, the prepared composite of TiO2/g-C_3N_4 demonstrated higher electrochemical capacitive behavior than pure TiO_2 and g-C_3N_4. This method provides a facile and straightforward approach for affixing porous TiO_2 NFs on the surface of g-C_3N_4 sheets from a simple and low cost electrospinning process.

EXPERIMENTAL

Materials

Commercially available g-C_3N_4 particles nicanite®, (Carbedon, Finland), acetic acid, titanium isopropoxide (TTIP), polyvinyl acetate (PVAc, Mw = 500000) and N,N-

Dimethylformamide (DMF) were purchased from Sigma Aldrich and used as-received.

Fabrication of TiO_2 NFs-intercalated g-C_3N_4 sheets

Here, TiO_2/g-C_3N_4 hybrid composite was directly prepared by using an angled two-nozzle electrospinning-calcination process. Typically, two different solutions, one containing g-C_3N_4 and the other containing TiO_2 precursors were made from the same polymer solution. First, PVAc solution (18 wt %) in DMF was prepared by overnight magnetic stirring at room temperature. Thereafter, g-C_3N_4 particles (1, 3, 5 and 10 wt % with respect to the weight of the PVAc) were added to the PVAc solution and the mixture was subjected to bath sonication for two hours, to disperse the g-C_3N_4 particles. Similarly, the TiO_2 precursor-containing PVAc solution was prepared by mixing 6g of the PVAc solution and 5 g of clear solution of TTIP (obtained by dropwise addition of acetic acid with continuous stirring). For two-nozzle electrospinning, one syringe contained PVAc solution with g-C_3N_4 particles while the other contained PVAc solution with TiO_2 precursors. The angle between the two nozzle tips was maintained at 80˚. A schematic diagram for the preparation of the composite is as shown in Figure 1. Electrospinning was carried out in room conditions where the parameters include 18 kV of applied voltage, a tip-to-collector distance of 12 cm, and solution feed rate of 1 ml/h. The obtained electrospun mats were vacuum dried at 80 ˚C overnight. Then the vacuum-dried electrospun mats were treated in air at 500 ˚C for 3h at the heating rate of 5 ˚C/min. At such a high temperature, TTIP [Ti {OCH (CH] molecules could decompose into TiO_2, CO_2 and H_2O. Here, CO_2 and H_2O escaped rapidly, and only TiO_2 and g-C_3N_4 sheets remained. At high temperature, TiO_2 molecules could react and generate anatase/rutile-TiO_2. Here, the composite material in which TiO_2 NFs attached on the surface of the g-C_3N_4 sheets are denoted as "TCN-x", where, "TCN" refers TiO_2/g-C_3N_4 composite and x refers the wt % of g-C_3N_4 w.r.t. the polymer weight, namely 1, 3, 5 and 10. Note that the mass ratio of g-C_3N_4 sheet affects the spinnability of the solution. Above 10 wt % of g-C_3N_4 sheet, spinnability diminishes and it is difficult to obtain fibers due to the increasing viscosity. Moreover, pristine TiO_2 NFs were prepared the same as TiO_2/g-C_3N_4 from the solution containing TiO_2 precursors, using a single-nozzle electrospinning process with all conditions identical to that of the two-nozzle electrospinning.

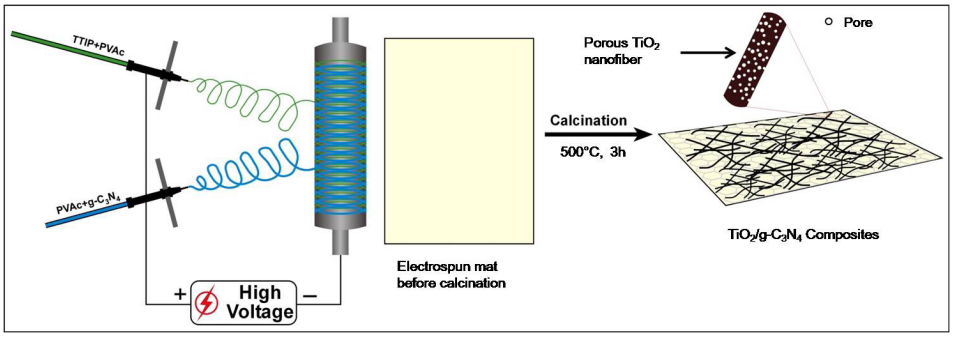

Figure 1: Schematic illustration for the synthesis of the TiO_2/g-C_3N_4 composite.

Electrochemical measurements

The cyclic voltammograms (CV) were taken in an N_2-saturated 0.01M potassium ferrocyanide solution prepared with 1M KNO_3, with the scanning rate 50 mV/s on a Potentiostat/Galvanostat/EIS (WonTech, ZIVE, SPI Korea) that was equipped with three-electrode system. A platinum electrode, 1.6 mm in diameter and coated with the as-prepared catalyst paste was used as the working electrode. A standard calomel electrode was used as the reference electrode and platinum wire was used as the counter electrode. Similarly, electrochemical impedance spectra (EIS) Nyquist plots measurements were taken in the same system over the frequency range of 0.001 to 100 kHz. Before measurement, the working electrode was prepared as follows: 20 mg of the different as-prepared samples were added to 20 μL of a solution of Nafion (5 wt %) and propanol. Subsequently, ultrasonication was carried out for 1 h to obtain a homogeneous paste. Then 5 μg of the paste was taken and dripped on the surface of the platinum electrode to form a thin catalyst film on the electrode. After drying at 80 ˚C in an oven for 30 min, the working electrode was used for experiments.

RESULTS AND DISCUSSION

Characterization of the composite

The morphologies of the prepared samples are observed by FE-SEM. It was found that TTIP/PVAc composite electrospun NFs are uniform with smooth surfaces before calcination (Figure 3a). It can be observed from the figure that the TiO_2 NFs remained as continuous structures with uniform diameters after calcinations. However, their average diameter was decreased slightly (Figure 3b). Furthermore, in the composite electrospun mat with g-C_3N_4 sheet, fibers with two different diameters can be distinguished; the larger-diameter fibers are the fibers of g-C_3N_4/PVAc; the smaller-diameter fibers are the fibers of TTIP/PVAc, as demonstrated in Figure 3c. It is noticeable on the FE-SEM image that the TiO_2 NFs are affixed on the g-C_3N_4 sheet after calcination in a reasonably unvarying manner (Figure 3d). The attached NFs have a length of several micrometers with porous structure, but the diameter varies from 40 nm up to 150 nm. In contrast to the NPs, such NFs of significant length promote direct and sufficient contact with g-C_3N_4 sheet, resulting in less agglomeration, hence, further enhancing the photodegradation efficiency. Moreover, such a very thin sheet, having large aspect ratios, high surface area and a stoichiometric N/C ratio, increase the transport of charges and reduce the recombination probability of photoexcited charge carriers.

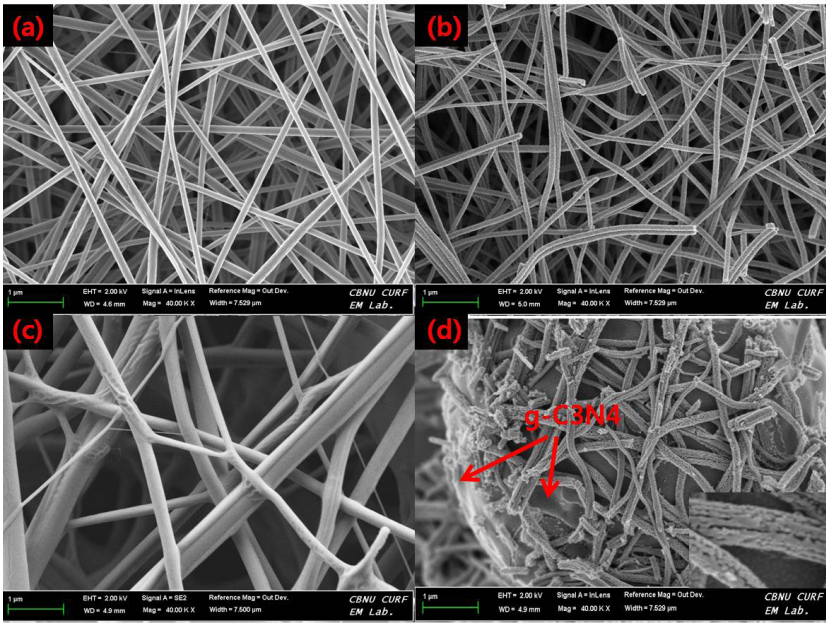

Figure 2: FE-SEM images of (a) TTIP/PVAC fibers before calcination, (b) TiO_2 fibers after calcination, (c) TTIP/PVAC/g-C_3N_4 fibers before calcination, and (d) TCN composite after calcinations (inset of figure d shows the porous structure of TiO_2 NFs).

The XPS survey spectrum and high resolution spectrum of the pristine and composite samples were carried out to further illuminate the surface composition and chemical interaction between the elements. Figure 3a illustrates the XPS survey spectrum of g-C_3N_4, TiO_2 and TCN. Obviously, the g-C_3N_4 contains the photoelectron peaks of C and N elements, and TCN-5 composite contains the photoelectron peaks of C, N, Ti and O elements. However, the pure TiO_2 NFs not only contain the photoelectron peaks of Ti and O elements, but also contains the peak of C elements. This carbon peak is ascribed to the residual carbon from the samples and adventitious hydrocarbon from the XPS instrument itself. The deconvoluted peaks of all elements of the composite material are given in the corresponding high-resolution spectrum (Figure 3b-3e). The C 1s peak of composite can be deconvoluted two fitted peaks at 285.65 eV and 287.05 eV (Figure 3b) indicating that carbon posses two diverse chemical states [23]. The peak around 285.65 eV is attributed to defects in the g-C_3N_4 that involves sp^2-hybridized carbon atoms. In addition, the other peak located around 287.05 eV is assigned to N—C═N coordination [24, 25]. The curves of N 1s region can be divided also into two peaks situated at 397.7eV and 399.8 eV (Figure 3c). The main peak located at 397.7eV belong to sp2 –hybridized pyridinic-like nitrogen(N-sp^2C) and the peak located at 399.8 eV corresponds to the tertiary pyrrolic graphitic nitrogen (N—$(C)_3$) [26]. The Ti $2p_{3/2}$ spin-orbital splitting photoelectron of the composite was located at binding energy 459.5 eV in the Ti 2p spectrum. Similarly, peaks at 465.05 eV in the same spectrum correspond to the Ti $2p_{1/2}$ (Figure 3d) [27]. The peak situated at 530.65 eV in the O 1s is ascribable to oxygen anions in the lattice (Ti-O)

(Figure 3e) [28]. Furthermore, the binding energy values of Ti 2p in the composite are slightly higher than those of pristine TiO_2 (Figure 3f) [29]. Hence, the results from FE-SEM and XPS analyses strongly verified that the TiO_2 NFs are attached on the surface of g-C_3N_4 sheets forming a hetero-structure rather than a physical mixture.

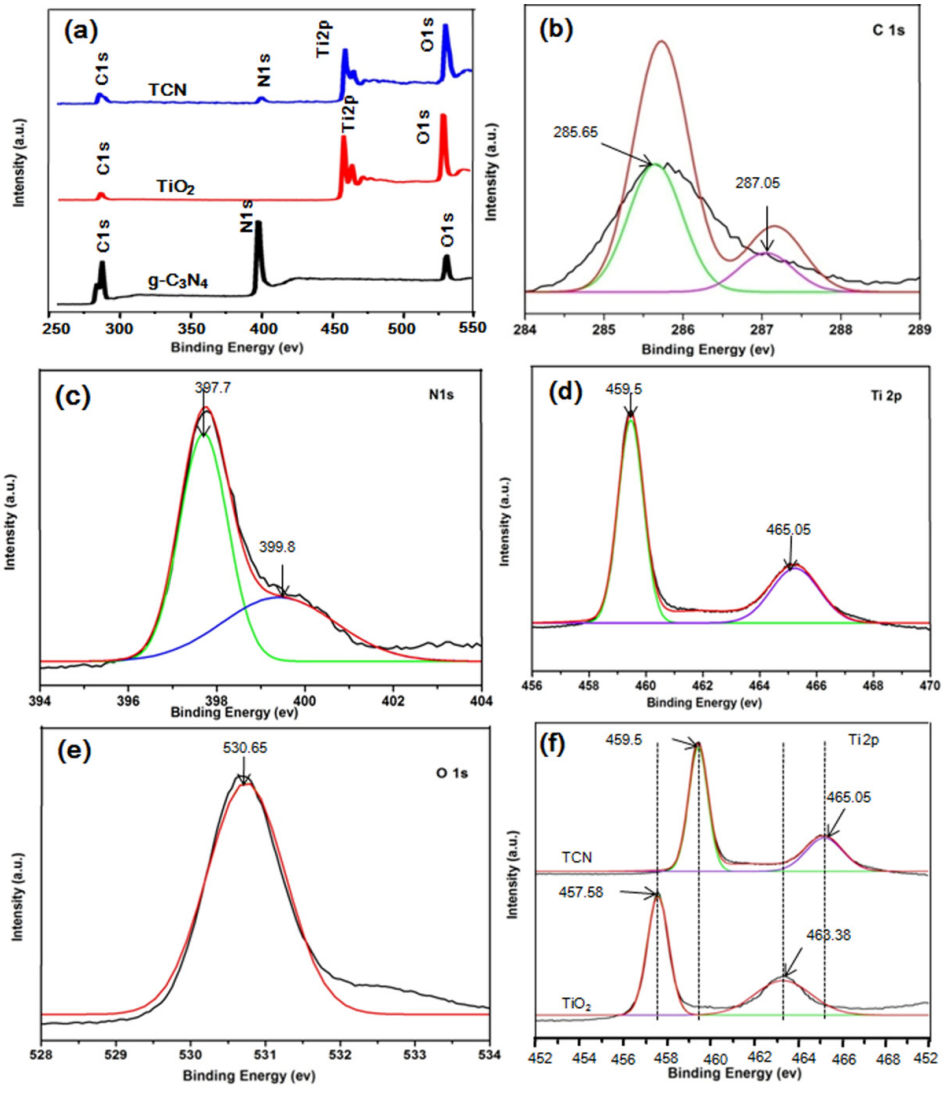

Figure 3: (a) XPS survey spectrum and high resolution XPS spectra of (b) C1s, (c) N1s, (d) Ti 2p, (e) O1s and (f) shifting of Ti2p peak in TCN-5 composite.

To analyze the electrochemical capacitive performance, a potentiostat/galvanostat/EIS analyzer was used to measure the CV to confirm the interfacial charge transfer effect of TiO_2, g-C_3N_4 and TCN-5. Figure 4 reveals CV of different samples, in which clearer reduction and oxidation peaks are observed for TCN-5 than other two pristine samples. As shown in the figure, the oxidation peaks for g-C_3N_4, TiO_2 and TCN-5 are located at

0.45, 0.57and 0.27 V and respectively represent the oxidation of ferrocyanide with the loss of one electron. The peak current of TCN-5 (0.127 mA/cm^2) is much higher than that of g-C_3N_4 (0.0505 mA/cm^2) and TiO_2 (0.039 mA/cm^2)-more than 2.5 times, signifying a considerably improved the capacitive performance. Furthermore, the ratio of the strengths of the oxidation (0.127 mA/cm^2, 0.29V) and reduction peaks (0.112 mA/cm^2, 0.15V) of TCN-5 is nearly 1, which specifying greatly enhanced reaction reversibility. The electrode capacitance depends on the CV curve area, scan rate, material amount and applied potential range. Here, TCN-5 has the highest specific area among the others, so the composite of TiO_2 and g-C_3N_4 electrode give the highest specific capacitance. EIS Nyquist plots were also recorded to further investigate the interfacial charge immigration of the samples (Fig.5). It has been reported in recent research that a smaller arc radius in Nyquist plots are related to a more effective interfacial charge immigration in semiconductor based electrode [30]. Arc radius for TCN-5 in the Nyquist plot (Figure 13) is smaller compared to g-C_3N_4 and TiO_2, demonstrating the reduced interface resistance so that the capacitive performance will be enhanced. Thus, combine with CV measurements and EIS Nyquist plots, it is concluded that the g-C_3N_4 sheet modified by porous TiO_2 NFs exhibits the enhanced capacitive performance compared to ones.

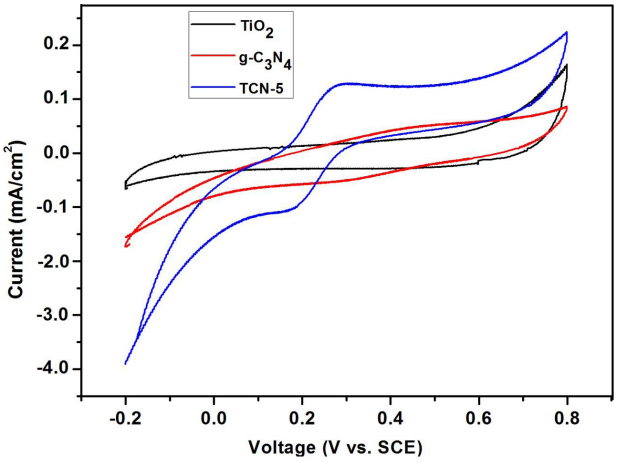

Figure 4: Cyclic voltammograms of TiO_2, g-C_3N_4 and TCN-5

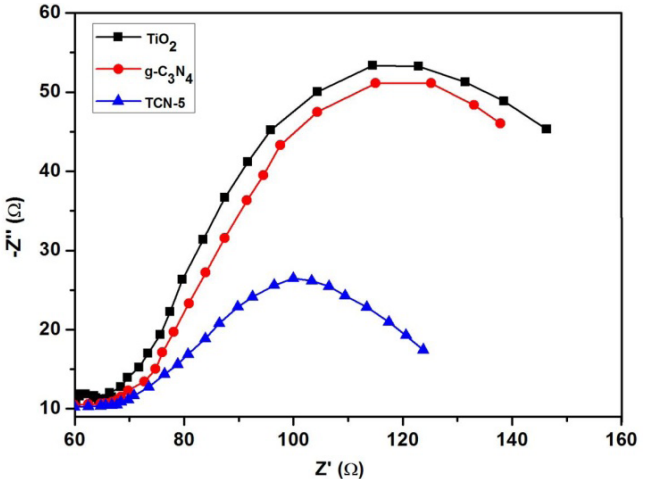

Figure 5: Electrochemical impedance spectra of TiO_2, g-C_3N_4 and TCN-5

Conclusions

In conclusion, we display a new technique to synthesize TiO_2 porous hollow NFs well attached to the surface of the sheet-like structure of g-C_3N_4 through the use of a simple and facile two nozzle electrospinning process followed by calcination process. Because of the hierarchical porous structure, the composite has relatively large specific surface area. The CV and EIS Nyquist plots measurements showed that, after incorporation of porous TiO_2 NFs, the composites exhibited significantly enhanced electrochemical capacitive performance compared to pristine TiO_2 and g-C_3N_4. Here the hollow one dimensional porous structure attached on the g-C_3N_4 sheet play an important role to enhance the capacitive performances of composite.

Acknowledgement

This research was supported by research fund of Chonbuk National University in 2014 and by grants from the Korean Ministry of Education, Science, and Technology (MEST) through the National Research Foundation (NRF) (Project no: 2014-R1A1A2009068)[2]

[1] *E. Conway B. Transition From Supercapacitor to Battery Behaviour in Electrochemical Energy-Storage1991.*

[2] *Jiang H, Lee PS, Li C. 3D carbon based nanostructures for advanced supercapacitors. Energy & Environmental Science 2013;6:41-53.*

[3] *Li Y, Xu X, He Y, Jiang Y, Lin K. Nitrogen Doped Macroporous Carbon as Electrode Materials for High Capacity of Supercapacitor2017.*

[4] *Pagketanang T, Artnaseaw A, Wongwicha P, Thabuot M. Microporous Activated Carbon from KOH-Activation of Rubber Seed-Shells for Application in Capacitor Electrode. Energy Procedia 2015;79:651-6.*

[5] *Zhou S-X, Tao X-Y, Ma J, Guo L-T, Zhu Y-B, Fan H-L, et al. Synthesis of flower-like PANI/g-C3N4 nanocomposite as supercapacitor electrode. Vacuum 2018;149:175-9.*

[6] *Abstracts. Fuel and Energy Abstracts 2014;55:2-98.*

[7] *Hou Y, Wen Z, Cui S, Feng X, Chen J. Strongly Coupled Ternary Hybrid Aerogels of N-deficient Porous Graphitic-C3N4 Nanosheets/N-Doped Graphene/NiFe-Layered Double Hydroxide for Solar-Driven Photoelectrochemical Water Oxidation. Nano Letters 2016;16:2268-77.*

[8] *LiZ, Wu L, Wang L, Gu A, Zhou Q. Nickel cobalt sulfide nanosheets uniformly anchored on porous graphitic carbon nitride for supercapacitors with high cycling performance. Electrochimica Acta*

2017;231:617-25.

[9] Tang L, Jia C-t, Xue Y-c, Li L, Wang A-q, Xu G, et al. Fabrication of compressible and recyclable macroscopic g-C3N4/GO aerogel hybrids for visible-light harvesting: A promising strategy for water remediation. Applied Catalysis B: Environmental 2017;219:241-8.

[10] Hou Y, Li J, Wen Z, Cui S, Yuan C, Chen J. N-doped graphene/porous g-C3N4 nanosheets supported layered-MoS2 hybrid as robust anode materials for lithium-ion batteries. Nano Energy 2014;8:157-64.

[11] Mamba G, Mishra AK. Graphitic carbon nitride (g-C3N4) nanocomposites: A new and exciting generation of visible light driven photocatalysts for environmental pollution remediation. Applied Catalysis B: Environmental 2016;198:347-77.

[12] Shi L, Zhang J, Liu H, Que M, Cai X, Tan S, et al. Flower-like Ni(OH)2 hybridized g-C3N4 for high-performance supercapacitor electrode material. Materials Letters 2015;145:150-3.

[13] Su C, Hong BY, Tseng CM. Sol–gel preparation and photocatalysis of titanium dioxide. Catalysis Today 2004;96:119-26.

[14] Nitnithiphrut P, Thabuot M, Seithtanabutara V. Fabrication of Composite Supercapacitor Containing Para Wood-derived Activated Carbon and TiO2. Energy Procedia 2017;138:116-21.

[15] Ren L, Li Y, Hou J, Zhao X, Pan C. Preparation and Enhanced Photocatalytic Activity of TiO2 Nanocrystals with Internal Pores. ACS Applied Materials & Interfaces 2014;6:1608-15.

[16] Height MJ, Pratsinis SE, Mekasuwandumrong O, Praserthdam P. Ag-ZnO catalysts for UV-photodegradation of methylene blue. Applied Catalysis B: Environmental 2006;63:305-12.

[17] Zhang Y, Zhang N, Tang Z-R, Xu Y-J. Graphene Transforms Wide Band Gap ZnS to a Visible Light Photocatalyst. The New Role of Graphene as a Macromolecular Photosensitizer. ACS Nano 2012;6:9777-89.

[18] Luo M, Liu Y, Hu J, Liu H, Li J. One-Pot Synthesis of CdS and Ni-Doped CdS Hollow Spheres with Enhanced Photocatalytic Activity and Durability. ACS Applied Materials & Interfaces 2012;4:1813-21.

[19] Sayama K, Hayashi H, Arai T, Yanagida M, Gunji T, Sugihara H. Highly active WO3 semiconductor photocatalyst prepared from amorphous peroxo-tungstic acid for the degradation of various organic compounds. Applied Catalysis B: Environmental 2010;94:150-7.

[20] Niu P, Zhang L, Liu G, Cheng H-M. Graphene-Like Carbon Nitride Nanosheets for Improved Photocatalytic Activities. Advanced Functional Materials 2012;22:4763-70.

[21] Pan X, Zhao Y, Liu S, Korzeniewski CL, Wang S, Fan Z. Comparing Graphene-TiO2 Nanowire and Graphene-TiO2 Nanoparticle Composite Photocatalysts. ACS Applied Materials & Interfaces 2012;4:3944-50.

[22] Han C, Wang Y, Lei Y, Wang B, Wu N, Shi Q, et al. In situ synthesis of graphitic-C3N4 nanosheet hybridized N-doped TiO2 nanofibers for efficient photocatalytic H2 production and degradation. Nano Res 2015;8:1199-209.

[23] Ng J, Wang X, Sun DD. One-pot hydrothermal synthesis of a hierarchical nanofungus-like anatase TiO2 thin film for photocatalytic oxidation of bisphenol A. Applied Catalysis B: Environmental 2011;110:260-72.

[24] Liu B, Zeng HC. Carbon Nanotubes Supported Mesoporous Mesocrystals of Anatase TiO2. Chemistry of Materials 2008;20:2711-8.

[25] Chai B, Peng T, Zhang X, Mao J, Li K, Zhang X. Synthesis of C60-Decorated SWCNTs (C60-d-CNTs) and Its TiO2-Based Nanocomposite with Enhanced Photocatalytic Activity for Hydrogen Production2012.

[26] Huang Za, Sun Q, Lv K, Zhang Z, Li M, Li B. Effect of contact interface between TiO2 and g-C3N4 on the photoreactivity of g-C3N4/TiO2 photocatalyst: (001) vs (101) facets of TiO2. Applied Catalysis B: Environmental 2015;164:420-7.

[27] Fu M, Liao J, Dong F, Li H, Liu H. Growth of g-C3N4 Layer on Commercial TiO2 for Enhanced Visible Light Photocatalytic Activity2014.

[28] Chen Y, Huang W, He D, Situ Y, Huang H. Construction of Heterostructured g-C3N4/Ag/TiO2 Microspheres with Enhanced Photocatalysis Performance under Visible-Light Irradiation. ACS Applied Materials & Interfaces 2014;6:14405-14.

[29] Zhang Z, Huang J, Zhang M, Yuan Q, Dong B. Ultrathin hexagonal SnS2 nanosheets coupled with g-C3N4 nanosheets as 2D/2D heterojunction photocatalysts toward high photocatalytic activity. Applied Catalysis B: Environmental 2015;163:298-305.

[30] Hong SJ, Lee S, Jang JS, Lee JS. Heterojunction BiVO4/WO3 electrodes for enhanced photoactivity of water oxidation. Energy & Environmental Science 2011;4:1781-7